



HAL
open science

Spin precession of light holes in the spin-orbit field of strained GaAs nanowires

D. Paget, T. Amand, H. Hijazi, A. C. H. Rowe, G. Monier, E. Gil, F. Cadiz,
C. Robert Goumet, Y. André

► **To cite this version:**

D. Paget, T. Amand, H. Hijazi, A. C. H. Rowe, G. Monier, et al.. Spin precession of light holes in the spin-orbit field of strained GaAs nanowires. *Physical Review B*, 2023, 108 (20), pp.205402. 10.1103/physrevb.108.205402 . hal-04273094


HAL Id: hal-04273094

<https://cnrs.hal.science/hal-04273094v1>

Submitted on 7 Nov 2023

HAL is a multi-disciplinary open access archive for the deposit and dissemination of scientific research documents, whether they are published or not. The documents may come from teaching and research institutions in France or abroad, or from public or private research centers.

L'archive ouverte pluridisciplinaire **HAL**, est destinée au dépôt et à la diffusion de documents scientifiques de niveau recherche, publiés ou non, émanant des établissements d'enseignement et de recherche français ou étrangers, des laboratoires publics ou privés.

Spin precession of light holes in the spin-orbit field of strained GaAs nanowiresD. Paget,¹ T. Amand,² H. Hijazi,³ A. C. H. Rowe,¹ G. Monier,³ E. Gil,³ F. Cadiz,¹ C. Robert Goumet,³ and Y. André³¹*Physique de la matière condensée, CNRS, Ecole Polytechnique, Institut Polytechnique de Paris, 91120 Palaiseau, France*²*Université de Toulouse, INSA-CNRS-UPS, LPCNO, 135 Avenue de Rangueil, 31077 Toulouse, France*³*Université Clermont Auvergne, Clermont Auvergne INP, CNRS, Institut Pascal, F-63000 Clermont-Ferrand, France* (Received 11 July 2023; revised 22 September 2023; accepted 16 October 2023; published 2 November 2023)

We have used a polarized spatially resolved microluminescence technique to investigate photocarrier charge and spin transport at 6 K in a GaAs nanowire (NW; n-type doping level $\approx 10^{17} \text{ cm}^{-3}$). Because of the difference in expansion coefficients of the NW and of its SiO_2 substrate, the NW is under strain, as revealed by the splitting between light- and heavy-hole emissions in the luminescence intensity spectrum. Light valence levels lie above the heavy valence ones, which is attributed as being caused by a tensile strain along both the axial and the lateral directions of the NW, equivalent to a compressive strain in the direction of light excitation. The symmetry group of the perturbed nanowire is then lowered to C_{2v} . No spin polarization can be evidenced for the heavy valence levels. The electron spin polarization decays up to a distance of 5 μm from the excitation spot, because of spin relaxation, and stays constant for larger distances because of the increased value of the drift velocity. Remarkably, the light-hole spin polarization exhibits damped spatial oscillations over as much as 5 μm . Analysis of the effect of strain on valence states shows that these oscillations are caused by the spin-orbit interaction in the light valence level. It is found that, for the C_{2v} point group, the corresponding Hamiltonian is linear in momentum. This spin-orbit interaction causes coherent oscillations rather than a spin relaxation process since transport essentially has a drift character in the internal electric field. The equivalent effective magnetic field induced by spin-orbit interaction and strain is, taking a light-hole g factor of 1, of the order of 60 mT.

DOI: [10.1103/PhysRevB.108.205402](https://doi.org/10.1103/PhysRevB.108.205402)**I. INTRODUCTION**

The effect of spin-orbit interaction on the electronic spin in the conduction band has been investigated in detail because of potential applications using the spin degree of freedom for information transfer [1–5]. In particular, the electron spin has been shown to exhibit precessions over long distances with limited losses caused by spin relaxation (the persistent spin helix) [6–10].

Hole spins are believed to be also highly interesting because of the larger spin-orbit interaction [11]. However, in bulk unstrained cubic semiconductors, the effect of the spin-orbit interaction on holes' spin is poorly known because of the very short hole spin relaxation time [12]. In GaAs-based quantum wells, the confinement removes the degeneracy between light- and heavy-hole states and has been shown to strongly increase the hole spin relaxation time [13,14]. Investigations of the spin properties have mostly been limited to those of heavy holes for which the corresponding electronic level in the valence band lies above that of light holes [11,15] and to theoretical investigations of the spin-dependent band structure [16] and of the spin-orbit-interaction-induced hole spin relaxation [17].

The breaking of cubic symmetry can also be induced by application of a uniaxial strain [18] or by strain induced by the lattice mismatch with the substrate [19,20]. This breaking has been shown to induce a significant modification of electronic features such as spin relaxation [18], spin-orbit splitting [21], and mobility [22]. However, only a very small number of studies have considered the effect of a strain on hole spins [23,24].

The present work is a theoretical and experimental investigation of the effect of a strain on valence hole states in n-doped nonquantizing GaAs nanowires (NWs). The strain originates from a difference between the thermal expansion coefficient of GaAs and that of its substrate. The splitting of the light and heavy valence bands is consistent with a biaxial symmetry breaking, both in the axial direction and in the lateral direction of the NW, rather than with a uniaxial breaking in the sole axial direction.

We show that light holes generated by a tightly focused light excitation are spin polarized and that their spin polarization exhibits damped spatial oscillations during spatial transport up to 5 μm from the excitation spot. In this case, a group theoretical analysis shows that the spin-orbit interaction acting on valence holes is linear in momentum and is able to induce a precession of the hole spin. As shown by self-consistent calculations, transport mostly has a drift character in the internal electric field. This unique feature enables the observation of coherent oscillations rather than inducing a relaxation process.

II. EXPERIMENT**A. Principles**

As shown in the inset of Fig. 1, we have chosen a NW of length 25 μm and diameter 90 nm. Such a NW, grown by hydride vapor phase epitaxy on a Si(111) substrate [25], lies on the metallic side of the Mott transition (n-type doping level $\approx 10^{17} \text{ cm}^{-3}$) [26] and has strong potentialities for electron charge and spin transport [27,28]. This NW is depleted since

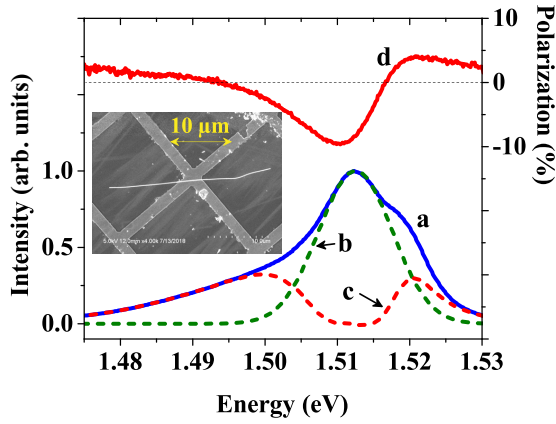


FIG. 1. Curve a shows the luminescence intensity spectrum at 6 K of a depleted NW at the excitation spot. The intensity spectrum exhibits a dominant component near 1.51 eV, shown by curve b, along with high- and low-energy shoulders, shown by the residual signal, curve c. Curve d shows the spectrum of the degree of circular polarization, given by Eq. (1). The presence of strains in the NW is revealed by the negative polarization near 1.51 eV, at which point recombination occurs to a split light-hole level. The inset shows an electron microscope image of the NW.

its diameter is smaller than the limit of 180 nm for this doping level [27].

After a surface passivation by an alkaline hydrazine sulfide solution [29], the NW was scraped and deposited horizontally on a grid of lattice spacing 15 μm . The NW was excited by a tightly focused, continuous-wave, σ^\pm -polarized laser beam (Gaussian radius $\approx 0.6 \mu\text{m}$) [30]. The excitation energy was 1.59 eV, thus enabling transitions from both heavy and light valence levels. Using a setup described elsewhere [27,31], the luminescence intensity I as a function of distance to the excitation spot was monitored, at a given energy in the spectrum and for a given distance from the excitation spot. Thus emission spectra could be recorded at a given distance from the excitation spot, as well as luminescence spatial profiles at a given energy in the spectrum. This latter investigation was performed using difference measurements with the laser spot on the NW and slightly out of the NW, thus resulting in a dynamic range larger than three orders of magnitude.

Using a σ^i circularly polarized excitation, where $i = \pm$, the intensity I_{ij} of the component of the luminescence with σ^j helicity ($j = \pm$) was also monitored. Here, in order to remove parasitic signals due to residual birefringence of components in the setup, we define the degree of polarization as the relative difference between copolarized and contrapolarized emission intensities

$$\mathcal{P} = \frac{1}{2I} [I_{++} + I_{--} - I_{+-} - I_{-+}]. \quad (1)$$

The value of \mathcal{P} is positive (negative) if the luminescence is copolarized (contrapolarized) with respect to the laser.

In order to obtain the expression for \mathcal{P} under strain, we show in Fig. 2 the optical transitions at $k = 0$, for excitation and recombination, for σ^\pm -polarized light. To first order, one assumes here, as is generally done, that the only effect of strain is to shift the valence levels, the light valence

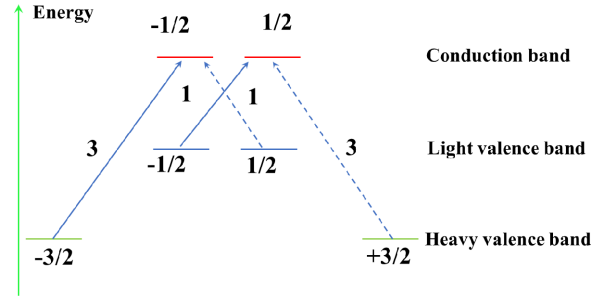


FIG. 2. Valence and conduction states at $k = 0$ for a strained semiconductor with light valence levels above the heavy ones. Solid (dashed) arrows show the transitions corresponding to $\Delta m = +1$ ($\Delta m = -1$) and to emission or absorption of a σ^+ -polarized (σ^- -polarized) photon. Also shown are the corresponding relative oscillator strengths.

level lying above the heavy one for a compressive strain [32]. The polarizations of electrons, light holes, and heavy holes are defined as $P_e = (n_{+1/2} - n_{-1/2}) / (n_{+1/2} + n_{-1/2})$, $P_{lh} = (p_{+1/2} - p_{-1/2}) / (p_{+1/2} + p_{-1/2})$, and $P_{hh} = (p_{+3/2} - p_{-3/2}) / (p_{+3/2} + p_{-3/2})$. Here, the electron, light-hole, and heavy-hole populations are $n_{\pm 1/2}$, $p_{\pm 1/2}$, and $p_{\pm 3/2}$, respectively [33]. The degree of circular polarization \mathcal{P}_{lh} (\mathcal{P}_{hh}) of the luminescence related to light (heavy) holes is given by

$$\begin{aligned} \mathcal{P}_{lh} &= \frac{P_e + P_{lh}}{1 + P_e P_{lh}} \approx P_e + P_{lh}, \\ \mathcal{P}_{hh} &= \frac{-P_e + P_{hh}}{1 - P_e P_{hh}} \approx -P_e + P_{hh}. \end{aligned} \quad (2)$$

The approximate expressions in the above equations are valid to first order since the spin polarizations are small with respect to unity. For a σ^+ -polarized light excitation, $P_e < 0$. Since a transition from a given valence level m leaves an excess hole of momentum $-m$, one has $P_{lh} > 0$ and $P_{hh} > 0$. Thus, since hole polarizations are usually smaller than the electron ones, one expects that the light-hole luminescence is contrapolarized with respect to the laser, while the heavy-hole luminescence is copolarized (i.e., $\mathcal{P}_{lh} < 0$ and $\mathcal{P}_{hh} > 0$). A contrapolarized emission has indeed generally been interpreted as related to a light-hole recombination [34].

Throughout this paper we shall use three orthonormal coordinate systems, defined by

$$\begin{aligned} x &= [100], & y &= [010], & z &= [001], \\ X &= \frac{1}{\sqrt{6}}[11\bar{2}], & Y &= \frac{1}{\sqrt{2}}[\bar{1}10], & Z &= \frac{1}{\sqrt{3}}[111], \\ x' &= \frac{1}{\sqrt{2}}[110], & y' &= \frac{1}{\sqrt{2}}[\bar{1}10], & z' &= [001]. \end{aligned} \quad (3)$$

The first orthonormal coordinate system is the usual frame for a cubic crystal. The second one is the natural system for a NW axis along the [111] crystal orientation. The third one will be used for strain along the [110] direction.

B. Intensity and polarization spectra at the excitation spot

Curve a in Fig. 1 shows the intensity spectrum taken at the excitation spot, at a lattice temperature of 6 K and for a weak excitation power of 45 μ W. The main line is approximated by a Gaussian profile of peak position 1.512 eV and half width 7.2 meV (curve b). As seen from curve c, the residual signal is the sum of a high-energy emission peaking at 1.520 eV and a low-energy tail. This tail is due to indirect recombination transitions in real space and will not be considered here [28,35,36].

Curve d in Fig. 1 shows the spectrum of the degree of circular polarization \mathcal{P} and reveals that the main line is contrapolarized with respect to the laser, while the high-energy component is copolarized. As seen from Eq. (2), where $P_e < 0$, $P_{lh} > 0$, and $P_{hh} > 0$, the only possible explanation for a contrapolarized emission is that this line is due to recombination with light holes. The conclusion that light holes are spin polarized cannot be drawn from the sole polarization spectrum but rather, as seen below, from the polarization spatial profiles. In agreement with Eq. (2), the copolarized high-energy component is caused by recombination with heavy holes. This implies that the light valence level lies above the heavy valence one, with a splitting of 8 meV.

Since the thermal expansion coefficient of GaAs ($6 \times 10^{-6} \text{ K}^{-1}$) is larger than that of the SiO₂ substrate ($0.6 \times 10^{-6} \text{ K}^{-1}$), the stress at low temperature is expected to be tensile along the plane of the substrate. This situation is similar to the case of GaAsN alloys deposited on GaAs [20] and is opposite to that of GaAs on CaF₂ substrates [19] and to quantum wells for which the heavy valence energy level lies above the light valence one.

The hypothesis of a tensile strain in the sole [111] NW axis cannot account for the results. Indeed, in this case and at variance with Fig. 2, the light valence level should lie below the heavy one (see Ref. [32]). Moreover, for circularly polarized light perpendicular to the NW axis, matrix elements for optical transitions between the heavy valence levels and the conduction band are zero for symmetry reasons [37]. This implies that, in contrast with experimental results, luminescence originated from recombination of spin-polarized conduction electrons with heavy valence levels should not be circularly polarized.

Here, one assumes that a tensile stress is also present in the direction perpendicular to the NW axis along which the NW is in contact with the substrate. The contact surface is nonzero since the NW is laterally faceted with probable facet orientations perpendicular to the X and Y crystallographic axes [38]. Assuming here that the contact is along X and Z , so that Y is the direction of optical excitation, the biaxial tensile stress along Z and X is equivalent to a compressive uniaxial stress along Y so that, in agreement with the experimental results, the light valence level lies above the heavy one. This situation is analogous to that found for GaAsN epilayers on GaAs [20], for which the luminescence and polarization spectra are very similar to those shown in Fig. 1, including a significant positive polarization of the heavy-hole emission and a lower energy of the light-hole luminescence. Within the C_{2v} symmetry group, diagonalization of the Hamiltonian

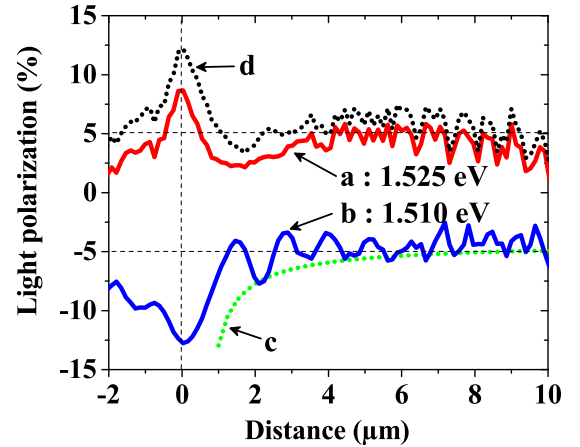


FIG. 3. Polarization spatial profiles at the light-hole (\mathcal{P}_{lh} ; curve b, 1.510 eV) and heavy-hole (\mathcal{P}_{hh} ; curve a, 1.525 eV) energies. Curve c, obtained using Eq. (11), is an estimate of the component P_e of curve b due to photoelectrons. The residual signal $\mathcal{P}_{lh} - P_e$ is due to spin-polarized light holes, for which the polarization exhibits damped oscillations during transport. Curve d is the spatial profile of \mathcal{P}_{hh} , obtained from curve a after correcting for the spectral admixture of the light-hole emission. This profile mostly exhibit features related to photoelectrons, without any visible contribution from heavy holes.

under strain [39] shows that the splitting at $k = 0$ is given by

$$\Delta = P \sqrt{B^2(S_{1,1} - S_{1,2})^2 + D^2 S_{4,4}^2}, \quad (4)$$

where $B \approx 2 \text{ eV}$ and $D \approx 5 \text{ eV}$ are energies characterizing the deformation potential tensor for light and heavy holes [40]. Here, the elasticity tensor coefficients $S_{1,1}$, $S_{1,2}$, and $S_{4,4}$ are given in Ref. [41]. From the value of the light-heavy valence splitting, we estimate that the pressure P is of the order of 0.9 kbar. This value is smaller than that of Ref. [20] by almost one order of magnitude.

C. Polarization spatial profiles

Curves a and b in Fig. 3 show the spatial profiles of the degree of circular polarization at energies of 1.525 and 1.510 eV, respectively. While curve b shows the spatial profile of \mathcal{P}_{lh} , the spatial profile of \mathcal{P}_{hh} is obtained from curve a by taking into account the residual light-hole-related emission at 1.525 eV. This profile is obtained by subtracting the quantity $\eta \cdot \mathcal{P}_{lh}$ as found from the luminescence line shape, $\eta \approx 0.3$, and is shown by curve d.

These spatial profiles are at variance with those of an unstrained depleted sample of similar diameter for which the polarization spatial profile is essentially flat [28]. Remarkably, \mathcal{P}_{lh} exhibits damped oscillations up to a distance of about 5 μ m from the excitation spot, while \mathcal{P}_{hh} essentially decreases up to $\approx 5\%$ at a distance of 3 μ m. The presence of oscillations on the spatial profile of \mathcal{P}_{lh} and their absence from that of \mathcal{P}_{hh} is remarkable. As seen from Eq. (2), this finding shows the following: (i) The oscillations concern the light-hole polarization rather than the conduction electron one. In the opposite case where the electron spin polarization oscillates, this would generate oscillations on both the heavy-

and light-hole emissions. (ii) An immediate consequence is that light holes are spin polarized and that the negative polarization of the main line has a significant negative contribution from light holes. For $Z \gtrsim 5 \mu\text{m}$ the oscillations have vanished, and one has $\mathcal{P}_{hh} = -\mathcal{P}_{lh} \approx 5\%$, as expected from Eq. (2) in the absence of hole polarization.

III. INTERPRETATION

We propose that, in the same way as found elsewhere for the conduction band [1,42], these oscillations originate from the spin-orbit interaction in the valence band.

A. The spin-orbit interaction under strain

Application of a strain strongly reduces the hole spin relaxation and is thus able to reveal the hole spin properties, including the effect of the hole spin-orbit interaction. This application also modifies the magnitude of the spin-orbit interaction, as shown in the Appendix, which gives, quite generally, the expressions of the terms linear and cubic in the momentum k and of the strain-dependent terms.

Here, as already performed by Durnev *et al.* [16] for quantum wells, we determine the hole spin-orbit Hamiltonian to lowest order in k by applying the method of invariants to the perturbed symmetry group (here C_{2v}) [39]. This method uses a decomposition of the Hamiltonian as the sum of several terms, each containing momentum operators and spin variables, and stipulates that a given matrix element of the spin-orbit Hamiltonian, being a scalar, must transform according to the Γ_1 representation of the C_{2v} point group. The valence band is split into two effective spin doublets which belong each to the same Γ_5^j ($j = l, h$) irreducible representation. The product $\Gamma_5 \otimes \Gamma_5 = \Gamma_1 + \Gamma_2 + \Gamma_3 + \Gamma_4$ contains the representations of the spin operator components $\hat{S}_y(\Gamma_2)$ and $\hat{S}_x(\Gamma_4)$. The wave-vector components k_x and k_y belong also to the Γ_2 and Γ_4 irreducible representations, respectively. Considering the reducible representation ($\Gamma_2 + \Gamma_4$) [one has $(\Gamma_2 + \Gamma_4) \otimes (\Gamma_2 + \Gamma_4) = 2\Gamma_1 + 2\Gamma_3$], we see that two independent constants are necessary to build an effective spin-orbit Hamiltonian (which must transform as a scalar). As the products $k_x \hat{S}_y$ and $k_x \hat{S}_x$ transform along the scalar representation Γ_1 , we determine at lowest order in \vec{k} the form of the effective spin-orbit Hamiltonian

$$\mathcal{H}_{so} = \frac{2}{\hbar} [\beta_{j2} k_x \hat{S}_{jy} + \beta_{j4} k_y \hat{S}_{jx}], \quad (5)$$

where the coefficients β_{j2} and β_{j4} are determined by the spin-orbit interaction and by the stress tensor. With respect to quantum wells on a $\bar{1}\bar{1}0$ substrate, this expression contains an additional term, depending on k_y [16]. For such quantum wells, this term is zero since $k_y = 0$ because of confinement.

In the XYZ frame, well adapted to the NW geometry, one obtains $\mathcal{H}_{so} = \mathbf{\Omega}_j \cdot \hat{S}$, where \hat{S} is the spin operator of light or heavy valence states and the precession vector is given by

$$\hbar \mathbf{\Omega}_j = \frac{2}{\sqrt{3}} \begin{pmatrix} \beta_{j4} k_y \\ \beta_{j2} (k_x + \sqrt{2} k_z) \\ \sqrt{2} \beta_{j4} k_y \end{pmatrix}. \quad (6)$$

Since without spin-orbit coupling, the hole spin is expected to lie along the direction Y of optical pumping, the presence of nonzero components of $\mathbf{\Omega}$ along X and Z , proportional to k_y , should cause a precession in an effective spin-orbit-interaction-related magnetic field.

B. Drift transport

In order to show that the spin-orbit interaction can generate oscillations, it is necessary to investigate the nature of transport in the NW. For usual diffusive transport, the fluctuations of k_y during the hole lifetime may decrease the coherence of the oscillations and also induce a spin relaxation process. Observation of coherent spatial oscillations also requires a nearly constant value of k_z , which is reached in the case of drift transport. In this case, possible fluctuations of k_x do not play a significant role since, in Eq. (6), k_x is negligible with respect to k_z .

The nature of transport in the NW is discussed here using the intensity spatial profiles, shown in the bottom panel of Fig. 4. Curve a (curve b), taken at the spectral position of the heavy (light) hole emission, reveals the spatial distribution of the intensity product np_h (np_l) of the photoelectron and heavy (light) hole concentrations. These two profiles are similar, suggesting the existence of a thermal equilibrium between light and heavy holes. They exhibit a rapid decrease up to $4 \mu\text{m}$ from the excitation spot and a slower decrease for larger distances [43].

The nonexponential nature of the intensity profile is analogous to spatial profiles in the case of ambipolar transport and reveals the existence of a significant internal electric field [44]. However, usual transport models, which assume electrical neutrality, would predict a negligible electric field since light holes and conduction electrons have a nearly equal effective mass [45]. In order to resolve this contradiction, it is pointed out that electrical neutrality is only strictly valid at zero temperature. For a nondegenerate electron-hole plasma at a nonzero temperature, thermal excitation of carriers induces a nonzero effective charge. In a volume of spatial extension L , the relative departure from neutrality is found, using Gauss's theorem, to be $(n - p)/n \approx (\lambda_D/L)^2$. Here, the Debye-Hückel length is $\lambda_D = \sqrt{\epsilon \epsilon_0 k_B T_e / (q^2 n)}$ [46], where k_B is Boltzmann's constant and T_e is the temperature of the photoelectron gas. Here, q is the absolute value of the electron charge, ϵ is the static dielectric constant, and ϵ_0 is the permittivity of the vacuum. The electric field E is then given by the very simple expression

$$E = \frac{k_B T_e}{qL}. \quad (7)$$

Taking $L = 4 \mu\text{m}$, which is the extension of the fast decrease and $T_e = 30 \text{ K}$, one finds $E \approx 7 \times 10^{-4} \text{ V}/\mu\text{m}$. It will be shown in the following section that, in this internal electric field, transport has a drift character.

IV. DISCUSSION

This section is devoted to a semiquantitative interpretation of the charge and polarization spatial profiles using a self-consistent numerical resolution.

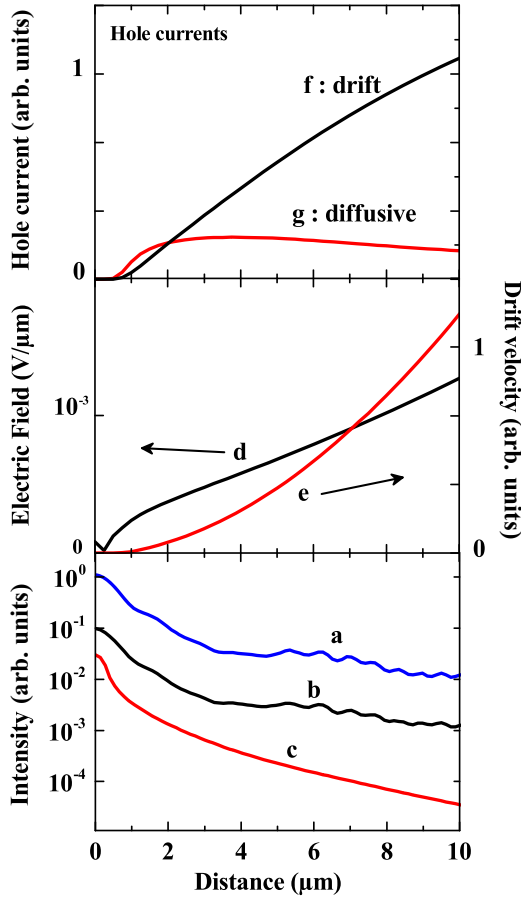


FIG. 4. The bottom panel shows the measured intensity spatial profiles at energies of 1.519 eV (heavy holes, curve a) and 1.510 eV (light holes, curve b). Curve c shows the calculated intensity profile, as explained in the text. Curve d in the middle panel shows the spatial profile of the internal electric field. Curve e in the middle panel shows the spatial profile of the carrier velocity, as obtained from the self-consistent calculations using Eq. (10). Curves f and g in the top panel show the spatial profiles of hole drift and diffusive currents. For a distance from the excitation spot larger than 2 μm , drift transport prevails over diffusive transport.

A. Interpretation of the intensity profiles

A key ingredient for transport in NWs slightly above the insulator-metal transition is the fact that, because of spatial statistical fluctuations of the donor concentration, the bottom of the conduction band and the top of the valence bands exhibit spatial energy fluctuations, so that transport occurs by hopping between the resulting potential wells. It has been found that transport in such a disordered system can be described by introducing a field dependence of the electron and hole mobilities, which, according to Refs. [47,48], take the form

$$\mu_{e(lh)}(E) = \mu_{e(lh)}^* \exp\left[-\frac{E_{e(lh)}}{|E|}\right], \quad (8)$$

where $\mu_{e(lh)}^*$ are the mobilities at large electric field. The characteristic electric fields $E_{e(lh)}$ are given by

$$E_{e(lh)} = \frac{\Delta_{e(lh)}}{q\delta}, \quad (9)$$

where the energies $\Delta_{e(lh)}$ are of the order of the fluctuation amplitude and δ is the length of an elementary tunnel process.

We have performed a self-consistent numerical resolution of the Poisson and drift diffusion equations, including Boltzmann statistics and imposing a zero potential at the NW ends and a zero recombination current at the lateral surfaces [28]. Because of the similar values of electron and light-hole effective masses, the electron and light-hole transport parameters were taken to be equal. The common values of $\mu_e^* = \mu_h^* = 6 \times 10^4 \text{ cm}^2 \text{ V}^{-1} \text{ s}^{-1}$ are a factor of 6 larger than those taken for an unstrained NW, in agreement with the reported mobility increase caused by application of a strain in a NW [22]. In the same way as for earlier work on unstrained NWs [28], we took $E_e = E_{lh} = 10^{-3} \text{ V}/\mu\text{m}$. The electron and hole lifetimes were $\tau = 3 \text{ ns}$. The values of the other parameters were found to have a negligible effect on the profile.

The calculated intensity spatial profile, shown by curve c in Fig. 4, is identical to the experimental one up to a distance of $\approx 5 \mu\text{m}$, i.e., in the range in which oscillations are observed. For larger distances, the decrease of the experimental profile is slightly slower than that of the experimental one. This has been observed before and could be caused by the onset of a quasiballistic hole transport regime in the increased electric field [28].

As shown by curve d in Fig. 4, the calculated internal electric field, of $6 \times 10^{-4} \text{ V}/\mu\text{m}$ at a distance of 4 μm , is comparable to the estimate using Eq. (7). Curve e in Fig. 4 shows the calculated spatial dependence of the electron drift velocity, given by

$$v_e = \mu_e^* E \exp\left(-\frac{E_e}{|E|}\right). \quad (10)$$

This velocity increases with distance because of the increase of both the electric field and the mobility. Curves f and g in Fig. 4 show the calculated spatial profiles of the hole drift and diffusive currents, respectively. While up to $\approx 2 \mu\text{m}$ transport is mostly diffusive, it has a drift character for larger distances. This is because for $z < 2 \mu\text{m}$, the internal electric field is smaller than E_e and E_h , so that, as seen from curve e in Fig. 4, the mobility and therefore the velocity are reduced. It is concluded that the spin oscillations occur during drift hole transport in the internal electric field.

B. Interpretation of the polarization spatial profiles

As seen from Eq. (6), the observation of coherent spatial oscillations suggests that k_Y is nearly constant during transport. A possible explanation may come from the value of the hopping range δ , given by Eq. (9), which plays the role of an effective mean free path. With the above value of E_e , one finds $\delta \approx 1 \mu\text{m}$, i.e., a value much larger than the NW radius. As a result, light holes localized in potential wells near the excitation spot have a larger probability of performing a hopping process along the Z direction than along the lateral ones. The quantity k_Y will thus be little modified, and will be approximately equal to its thermal value, so that the spin-orbit interaction produces a precession rather than a spin relaxation.

As seen from Eq. (2), the shape of the spatial profile of \mathcal{P}_{lh} suggests that its electronic contribution P_e decreases with increasing distance to the excitation spot and stays constant for distances larger 4 μm . This finding can be interpreted since, as shown by curve e in Fig. 4, the velocity increases with distance to the excitation spot because of the increase of the electric field. There results a decrease at large distance of the polarization losses by spin relaxation per traveled distance. A simple calculation shows that the spatial profile of the photoelectron spin polarization is given by

$$P_e(Z) = P_e(Z_0) \exp \left[- \int_{Z_0}^Z \frac{1}{v_e T_1} dl \right], \quad (11)$$

where Z is the distance to the excitation spot. For the spin relaxation time, we have taken $T_1 = 20$ ns, which is the value for unstrained material of the same doping [49] multiplied by a factor of ≈ 3 because of the strain-induced increase [18]. Here, the lower integration limit ($Z_0 = 1$ μm) is nonzero since transport near the excitation spot has been shown to be diffusive. We have chosen $P_e(Z_0) = -13\%$. The calculated spatial profile of $P_e(Z)$, shown by curve c in Fig. 3, coincides very well with the minima of \mathcal{P}_{lh} .

By difference, one finds that the spatial oscillations of the light-hole polarization P_{lh} are characterized by a spatial period of about 1.1 μm . As shown by curve d in Fig. 3, the spatial profile of \mathcal{P}_{hh} does not exhibit oscillations. One observes an initial rapid decay due to the photoelectron contribution, with an essentially flat profile at larger distances. This implies that no contribution of heavy holes to the luminescence circular polarization can be evidenced. The apparently weak spin polarization of heavy holes does not originate from a longer lifetime, as seen from the identical intensity spatial profiles, but rather from a smaller value of the heavy-hole spin relaxation time with respect to the light-hole one.

Finally, the magnitude of the spin-orbit interaction is estimated from the value of the drift velocity for which the calculated spatial profile is shown by curve e in Fig. 4. The time period of the oscillations is found to be of the order of 1 ns, and taking a light-hole g factor of 1, the spin-orbit interaction is found to correspond to an effective magnetic field of the order of 60 mT. Using the thermal value of k , one also finds that the coefficients βlh which appear in Eq. (6) are of the order of several 10^{-12} eV cm.

V. CONCLUSION

In conclusion, investigation of the charge and spin spatial profiles in a depleted GaAs NW under strain gives us a unique opportunity to study light-hole dynamics during transport. The polarization spectrum at the place of excitation shows that, at variance with most investigations on quantum wells and strained materials, (i) the light valence level lies above the heavy one and (ii) electrons as well as light holes are spin polarized. Drift transport in an internal electric field caused by a slight departure from charge neutrality leads to spatial oscillations of the light-hole mean spin, equivalent to precession in an effective magnetic field of ≈ 60 mT.

Using a theoretical description of the effect of a strain on the valence band, it is found that the ordering of heavy and light valence levels rather suggests a biaxial tensile strain,

equivalent to a compressive strain along the axis of light excitation, implying that the crystal point group of the strained NW is C_{2v} . In this case, the spin-orbit Hamiltonian acting on holes is linear in the momentum k and is consistent with the appearance of oscillations.

Note, finally, that the present NWs are not far from an optimum system, as a function of the characteristic dimension in the direction Y of light excitation, for observation of spin-orbit-interaction-related oscillations. For a very thin, quantizing NW or for a quantum well on a $[1\bar{1}0]$ substrate, the momentum k_Y has a zero value. Thus Ω given by Eq. (6) is perpendicular to the nanowire axis or to the plane of the quantum well, i.e., parallel to the initial spin polarization, so that, in agreement with Ref. [16], no spin precession will be observed. Conversely, for a lateral dimension larger than the typical length of an elementary hopping process, the quantities k_Y and k_X will fluctuate during transport, so that the spin-orbit interaction should induce a spin relaxation rather than coherent oscillations.

ACKNOWLEDGMENTS

We are grateful to V. L. Berkovits and P. A. Alekseev for advice regarding the chemical surface passivation. This work was supported by Région Auvergne-Rhône-Alpes (Pack Ambition Recherche; Convention 17 011236 01-61617, CPERMMASYF and LabExIMobS3 (ANR-10-LABX-16-01). It was also funded by the program Investissements d'Avenir of the French ANR agency, by the French government IDEX-SITE initiative 16-IDEX-0001 (CAP20-25), and by the European Commission (Auvergne FEDER funds). This work was supported by the International Research Center "Innovation Transportation and Production Systems" of the I-SITE CAP 20-25.

APPENDIX: HOLE SPIN-ORBIT HAMILTONIAN FOR UNSTRAINED AND STRAINED SEMICONDUCTORS

The spin-orbit Hamiltonian for unstrained cubic semiconductors has been described in Ref. [40]. Adopting the same method as used in Ref. [18] for conduction electron spins in a strained cubic material, we determine the linear-in- k and cubic-in- k components as follows. The nonrelativistic term is determined by symmetry and depends on the hole angular momentum \hat{J} . It is given by

$$\mathcal{H}_{v3} = [\gamma_{v3} \kappa(\mathbf{k}) + \gamma_{v3\epsilon} \kappa(\mathbf{k}, \vec{\epsilon}) + \gamma'_{v3\epsilon} \kappa'(\mathbf{k}, \epsilon')] \cdot \hat{J}, \quad (A1)$$

where γ_{v3} , $\gamma_{v3\epsilon}$, and $\gamma'_{v3\epsilon}$ are scalars and κ_{v3} , $\kappa_{v3\epsilon}$, and $\kappa'_{v3,\epsilon}$ are vectors of components along x , given by $\kappa_{v3x} = k_x(k_y^2 - k_z^2)$, $\kappa_{v3\epsilon x} = k_x(\epsilon_{yy} - \epsilon_{zz})$, and $\kappa'_{v3\epsilon x} = \epsilon_{xy}k_y - \epsilon_{xz}k_z$. The other components are obtained by cyclic permutation. Here, ϵ_{ij} are the components of the deformation tensor $\vec{\epsilon}$, and $\epsilon'_x = \epsilon_{yz}$ and the other components are obtained by cyclic permutations. Thus, for a zero strain, only the first term is present in the above equation, so that the second and third terms are additional strain-induced contributions to the nonrelativistic term. The spin-orbit interaction introduces a relativistic term, given by

$$\mathcal{H}_{v3}^{so} = [\gamma_{v3}^{so} \kappa(\mathbf{k}) + \gamma_{v3\epsilon}^{so} \kappa(\mathbf{k}, \vec{\epsilon}) + \gamma'_{v3\epsilon}^{so} \kappa'(\mathbf{k}, \epsilon')] \cdot \hat{J}. \quad (A2)$$

This term is of the same type as Eq. (A1), where the coefficients γ_{v3} , $\gamma_{v3\epsilon}$, and $\gamma'_{v3\epsilon}$ are replaced by γ_{v3}^{so} , $\gamma_{v3\epsilon}^{so}$, and $\gamma'_{v3\epsilon}^{so}$, respectively.

There is, finally, a term linear in momentum and strain, of the form

$$\mathcal{H}_{v1}^{so}(\mathbf{k}) = \frac{4}{3} [k_0^{so} \mathbf{k} + k_{0,\epsilon}^{so} \boldsymbol{\epsilon}] \cdot \hat{\mathbf{V}}, \quad (\text{A3})$$

where the components of the vector $\hat{\mathbf{V}}$ are given by $V_x = [J_x, (J_y^2 - J_z^2)]_+$, and cyclic permutations. Here, $[A, B]_+ = [AB + BA]/2$. In the same way as for the above equations, we have introduced a term dependent on the strain.

The form of these equations shows that strain strongly modifies the spin-orbit coupling, without, however, modifying its structure. It can be shown that to first order in k , the above expressions lead to Eq. (5).

-
- [1] M. W. Wu, J. H. Jiang, and M. Q. Weng, *Phys. Rep.* **493**, 61 (2010).
- [2] I. Zutic, J. Fabian, and S. D. Sarma, *Rev. Mod. Phys.* **76**, 323 (2004).
- [3] M. I. D'yakonov and V. I. Perel, *JETP Lett.* **13**, 467 (1971).
- [4] G. Wang, B. L. Liu, A. Balocchi, P. Renucci, C. R. Zhu, T. Amand, C. Fontaine, and X. Marie, *Nat. Commun.* **4**, 2372 (2013).
- [5] H. C. Koo, J. H. Kwon, K. Eom, J. Chang, S. H. Han, and M. Johnson, *Science* **325**, 1515 (2009).
- [6] M. Kohda and G. Salis, *Semicond. Sci. Technol.* **32**, 073002 (2017).
- [7] J. D. Koralek, C. Weber, J. Orenstein, A. Bernevig, Z. S. Mack, and D. Awschalom, *Nature (London)* **458**, 610 (2009).
- [8] F. Passmann, S. Anghel, C. Ruppert, A. D. Bristow, A. V. Poshakinskiy, S. A. Tarasenko, and M. Betz, *Semicond. Sci. Technol.* **34**, 093002 (2019).
- [9] V. K. Kalevich and V. L. Korenev, *Pis'ma Zh. Eksp. Teor. Fiz.* **52**, 230 (1990).
- [10] M. P. Walser, C. Reichl, W. Wegscheider, and G. Salis, *Nat. Phys.* **8**, 757 (2012).
- [11] B. Habib, M. Shayegan, and R. Winkler, *Semicond. Sci. Technol.* **24**, 064002 (2009).
- [12] D. J. Hilton and C. L. Tang, *Phys. Rev. Lett.* **89**, 146601 (2002).
- [13] Ph. Roussignol, P. Rolland, R. Ferreira, C. Delalande, G. Bastard, A. Vinattieri, J. Martinez-Pastor, L. Carraresi, M. Colocci, J. F. Palmier, and B. Etienne, *Phys. Rev. B* **46**, 7292(R) (1992).
- [14] X. Marie, T. Amand, P. Le Jeune, M. Paillard, P. Renucci, L. E. Golub, V. D. Dymnikov, and E. L. Ivchenko, *Phys. Rev. B* **60**, 5811 (1999).
- [15] R. Winkler, D. Culcer, S. J. Papadakis, B. Habib, and M. Shayegan, *Semicond. Sci. Technol.* **23**, 114017 (2008).
- [16] M. V. Durnev, M. M. Glazov, and E. L. Ivchenko, *Phys. Rev. B* **89**, 075430 (2014).
- [17] L. Wang and M. W. Wu, *Phys. Rev. B* **85**, 235308 (2012).
- [18] M. I. D'yakonov, V. A. Marushchak, V. I. Perel', and A. N. Titkov, *Sov. Phys. JETP* **63**, 655 (1986).
- [19] L. R. Tessler, C. Hermann, G. Lampel, Y. Lassailly, C. Fontaine, E. Daran, and A. M. Yague, *Appl. Phys. Lett.* **64**, 895 (1994).
- [20] A. Y. Egorov, V. K. Kalevich, M. M. Afanasiev, A. Y. Shiryaev, V. M. Ustinov, M. Ikezawa, and Y. Masumoto, *J. Appl. Phys.* **98**, 013539 (2005).
- [21] Y. K. Kato, R. C. Myers, A. C. Gossard, and D. D. Awschalom, *Nature (London)* **427**, 50 (2004).
- [22] L. Balaghi, S. Shan, I. Fotev, F. Moebus, R. Rana, T. Venanzi, R. Hübner, T. Mikolajick, H. Schneider, M. Helm, A. Pashkin, and E. Dimakis, *Nat. Commun.* **12**, 6642 (2021).
- [23] B. Habib, J. Shabani, E. P. DePoortere, M. Shayegan, and R. Winkler, *Phys. Rev. B* **75**, 153304 (2007).
- [24] X. Linpeng, T. Karin, M. V. Durnev, M. M. Glazov, R. Schott, A. D. Wieck, A. Ludwig, and K.-M. C. Fu, *Phys. Rev. B* **103**, 115412 (2021).
- [25] H. Hijazi, V. G. Dubrovskii, G. Monier, E. Gil, C. Leroux, G. Avit, A. Trassoudaine, C. Bougerol, D. Castellucci, C. Robert-Goumet, and Y. André, *J. Phys. Chem. C* **122**, 19230 (2018).
- [26] M. Benzaquen, D. Walsh, and K. Mazuruk, *Phys. Rev. B* **36**, 4748 (1987).
- [27] H. Hijazi, D. Paget, G. Monier, G. Grégoire, J. Leymarie, E. Gil, F. Cadiz, C. Robert-Goumet, and Y. André, *Phys. Rev. B* **103**, 195314 (2021).
- [28] H. Hijazi, D. Paget, A. C. H. Rowe, G. Monier, K. Lahlil, E. Gil, A. Trassoudaine, F. Cadiz, Y. André, and C. Robert-Goumet, *Phys. Rev. B* **105**, 195204 (2022).
- [29] P. A. Alekseev, M. S. Dunaevskiy, V. P. Ulin, T. V. Lvova, D. O. Filatov, A. V. Nezhdanov, A. I. Mashin, and V. L. Berkovits, *Nano Lett.* **15**, 63 (2015).
- [30] The excitation spot was at 7 μm from the left NW end, which leaves a straight NW section of 15 μm length. The metallic stripes lying on the NW substrate are found not to modify the intensity and polarization spatial profiles.
- [31] I. Favorskiy, D. Vu, E. Peytavit, S. Arscott, D. Paget, and A. C. H. Rowe, *Rev. Sci. Instrum.* **81**, 103902 (2010).
- [32] M. I. D'yakonov and V. I. Perel, *Sov. Phys. Semicond.* **7**, 1551 (1974).
- [33] We consider here valence states, of wave functions $|3/2, m\rangle$. The wave functions of the corresponding hole states are obtained by time reversal and given by $|3/2, m\rangle^h = (-1)^{3/2-m} |3/2, m\rangle$.
- [34] C. Weisbuch, R. C. Miller, R. Dingle, A. C. Gossard, and W. Wiegmann, *Solid State Commun.* **37**, 219 (1981).
- [35] A. L. Efros, Y. S. Halpern, and B. I. Shklovsky, in *Proceedings of the Eleventh International Conference on the Physics of Semiconductors, Warsaw 1972* (Polish Scientific, Warsaw, 1972), p. 126.
- [36] B. I. Shklovskii and A. L. Efros, *Electronic Properties of Doped Semiconductors* (Springer-Verlag, Berlin, 1984).
- [37] Because of the lowering of the crystal symmetry from T_d to C_{3v} caused by the application of a strain along [111], it can be shown that the heavy valence levels transform like the Γ_5 and Γ_6 representations of C_{3v} (see Ref. [50]), that the conduction levels transform like Γ_4 , and that the operator $p_x - ip_y$ for excitation by circularly polarized light transforms like Γ_3 . Here,

- \bar{p} is the electron momentum operator. The zero value of the corresponding matrix elements follows from the coupling tables [50].
- [38] V. Pankoke, P. Kratzer, and S. Sakong, *Phys. Rev. B* **84**, 075455 (2011).
- [39] G. L. Bir and G. E. Pikus, *Symmetry and Strain-Induced Effects in Semiconductors* (Wiley, New York, 1974).
- [40] E. L. Ivchenko and G. E. Pikus, *Superlattices and Other Heterostructures: Symmetry and Optical Phenomena*, Springer Series in Solid-State Sciences (Springer, New York, 1997).
- [41] A. Gavini and M. Cardona, *Phys. Rev. B* **1**, 672 (1970).
- [42] A. Balocchi, Q. H. Duong, P. Renucci, B. L. Liu, C. Fontaine, T. Amand, D. Lagarde, and X. Marie, *Phys. Rev. Lett.* **107**, 136604 (2011).
- [43] Note that spatial fluctuations of the intensity are superimposed on the profile and are similar for curves a and b in Fig. 3. Such fluctuations are not visible for a larger NW diameter [27]. We believe that they are caused by incomplete averaging of the disorder, so that the parameters for recombination and transport may slightly vary as a function of distance to the excitation spot.
- [44] D. Paget, F. Cadiz, A. C. H. Rowe, F. Moreau, S. Arscott, and E. Peytavit, *J. Appl. Phys.* **111**, 123720 (2012).
- [45] R. A. Smith, *Semiconductors* (Cambridge University Press, Cambridge, 1978).
- [46] K. Wiesemann, in *Lectures of the CAS-CERN Accelerator School: Ion Sources, Senec, Slovakia, 29 May – 8 June 2012*, edited by R. Bailey, CERN Yellow Report CERN-2013-007 (European Organization for Nuclear Research, Meyrin, Switzerland, 2014), pp. 85–122.
- [47] S. Baranovskii and O. Rubei, in *Springer Handbook of Electronic and Photonic Materials*, edited by S. Kasap and P. Capper (Springer-Verlag, Berlin, 2017), Chap. 9, pp. 195–216.
- [48] B. Cleve, B. Hartenstein, S. D. Baranovskii, M. Scheidler, P. Thomas, and H. Baessler, *Phys. Rev. B* **51**, 16705 (1995).
- [49] R. I. Dzhioev, K. V. Kavokin, V. L. Korenev, M. V. Lazarev, B. Y. Meltser, M. N. Stepanova, B. P. Zakharchenya, D. Gammon, and D. S. Katzer, *Phys. Rev. B* **66**, 245204 (2002).
- [50] G. F. Koster, R. G. Wheeler, J. D. Dimmock, and H. Statz, *Properties of the Thirty-Two Point Groups* (MIT Press, Cambridge, 1963).